



Improving tensile strength, impact toughness and wear resistance of TIG welded dissimilar AA7075-T6/AA6061-T6 joints through friction stir processing

Md Saquib Bin Reyaz¹ · Amar Nath Sinha¹

Received: 30 September 2023 / Accepted: 24 November 2023 / Published online: 17 January 2024
© The Author(s), under exclusive licence to Springer-Verlag France SAS, part of Springer Nature 2024

Abstract

Excellent strength and corrosion resistance make dissimilar AA6061-T6/AA7075-T6 aluminium welding a popular choice in the aviation and automobile industries. Fusion welding may lead to defects like voids, thermal cracks, residual stresses, and coarse grains, which can affect the integrity of the joints. To address these problems, friction stir processing (FSP) was commonly employed to increase the microstructural and mechanical features. This study examined the influence of tool spindle speeds on tungsten inert gas (TIG) welded joints, as well as the microstructural features and their relationship to tensile strength, impact toughness, and wear resistance. As the spindle speed of the tool increased, the dendritic coarse grain structure of TIG-welded joints in the fusion area transformed into equiaxed ultrafine structures in the stir region. For the TIG + FSP welded sample at 1300 rpm, the average grain size decreased by 83.10% and the tensile strength and impact toughness increased by 74.84 and 88.89%, respectively, while the wear rate decreased by 46.87%. The TIG + FSP joint had a high tensile strength of 278 MPa, a good impact toughness of 17 J, and a low wear rate of 86 μm at a tool spindle speed of 1300 rpm, while the TIG welded joint had a lower tensile strength of 159 MPa, an impact toughness of 9 J, and a higher wear rate of 132 μm . The tensile fractured surface of TIG joints showed rough cleavage facets, coarse dimples with some voids, while the TIG + FSP joints showed a fine equiaxed dimples with no voids.

Keywords TIG + FSP · Dissimilar aluminum plates · Scan electron microscopy · Energy diffraction scanning · Impact toughness · Wear resistance

1 Introduction

Friction stir processing (FSP) is derived from friction stir welding (FSW), which is a solid-state joining technique initially created for aluminium metals [1]. The FSP enhances the material's surface qualities via strong plastic deformation, mixing, and breaking the material via stirring action, and frictional heat generation [2, 3]. This innovative metalworking method alters and manages microstructures in the close-to-surface regions of metal parts. It enhances the mechanical features of the joint while eradicating flaws stemming from heat dispersion [4, 5]. The mechanical features encompass microhardness, impact toughness, flexural

strength, tensile strength, and percent elongation [6–8]. Over the years since its introduction, FSP has found diverse applications in enhancing the tensile properties of various materials, such as aluminum alloys. Beyond excelling in modifying material surfaces, FSP has also garnered attention for its recent contributions to improving the characteristics of previously welded joints, including friction stir welded and fusion welded joints, among others [9].

The FSP approach is strongly advised for enhancing the processed zone for multiple reasons. The metallurgical features of the friction stir processed area can be influenced by adjusting the tilt angle, tool spindle speed, traverse speed, and vertically pressure [10–12]. Other material processing techniques can be utilized, but the FSP technique stands out as the sole method that allows for control of processed depth by controlling the tool pin length. Additionally, friction stir processing is an eco-friendly method of processing that is energy-efficient. It is a completely automated process that offers excellent dimensional stability [13–15].

✉ Md Saquib Bin Reyaz
mdr.phd19.me@nitp.ac.in

¹ Department of Mechanical Engineering, National Institute of Technology Patna, Patna, Bihar 800005, India

Various kinds of literature concur with the support for FSP as a means to enhance the quality of fusion welds, including those produced through FSW. The study determined the use of the FSP technique on TIG welds of dissimilar AA6061 and AA7075 alloys with Si and Mg rich fillers to enhance mechanical strength and wear resistance [16]. It was deduced that as the Mg rich filler resulted in improved mechanical strength and wear resistance and lower residual stresses of the TIG weld. A significant grain refinement was observed for TIG + FSP welds, specifically the stir zone grain size reached to 3.2–4 μm . The tensile fractured surface of TIG welds exhibited cleavage facets, tear ridges and coarse dimples resulting brittle mode of failure, while the TIG + FSP welds showed fine and equiaxed dimples resulting ductile mode of failure for both the fillers. In another investigation, the friction stir processing was applied to the TIG welded joints of the above-mentioned alloys with same fillers and investigated the material flow and mechanical behaviour of the weldments [17]. The TIG welded joint exhibited high compressive residual stress values of the order 64 MPa at the fusion region for Si rich filler, while the TIG + FSP joint shown to be least compressive residual stress values of the order 39 MPa at stir region of the joint. The mechanical features of the TIG + FSP weldment were also increased due to the better material flow, significant grain refinement and existence of fine precipitates across the weld processed region. The FSP impact was added to the literature through the creation of statistical equations aimed at forecasting the mechanical characteristics and residual stress in the joint study mentioned earlier [18]. It was deduced that, TSS was the most influential factor that affected the TIG + FSP joint and found that improved mechanical features including tensile strength, % elongation, and microhardness compared to the TIG welded joint for increased spindle speeds. The mechanical characteristics were enhanced as a result of grain size reduction in the processed region owing to an elevated tool spindle speed. Thakral et al. [19] performed the friction processing to the TIG welded AA6061-T6 butt joints and investigated its effect on joint tensile and microhardness properties. They obtained a fine equiaxed recrystallized grains in the weld zone and improved tensile and microhardness properties after FSP. Da Silva et al. [20] conducted research into how FSP affects aluminum joints that have been MIG-welded, examining cases with and without additional reinforcements. The findings showed that FSP enhanced the fatigue life of the MIG welds, regardless of the presence of reinforcements. However, the hardness and mechanical strength were not significantly affected by FSP, although there was a slight improvement in ductility. Weak wetting and porosity in the MIG welded joints were identified as the root cause of the improvement. MIG + FSP junctions that included reinforcements had a finer grain size than those that did not. As a

result, the MIG + FSP joints that included reinforcements had better tensile properties. Saad et al. [21] performed FSP on the tungsten inert gas weldments of base AA7020 plate butt joints and found that the hardness strength of the joint improved by 118.5% over the TIG joints and by 103% over the base AA7020 plate. In another work on improving the MIG welded dissimilar 5083-H321/5356 aluminum joints using FSP have been documented in publications [22]. It was investigated that FSP led to enhanced grain-size strengthening, resulting from both grain refinement and the Hall–Petch relationship. Additionally, FSP demonstrated improved precipitate strengthening as a result of the breakdown and higher volume fraction of precipitates formed, which resulted in increased yield strength of the joint. This investigation utilized dissimilar AA6061-T6 and AA7075-T6 plates, both members of the heat treatable 6xxx and 7xxx aluminum alloy series. AA6061-T6, enriched with Al–Mg–Si, and AA7075-T6, comprising Al–Mg–Zn, have risen to prominence as fundamental structural aluminum alloys. AA6061-T6 finds application in motor vehicles, storage vessels, naval sections, pipes, and aviation frames, and various other industries, while AA7075-T6 is predominantly employed in the fields of aerodynamic elements, machined and arch components, exterior face components, and string-formed sections [23, 24]. With the growing utilization of various materials in industries like aerospace and automotive engineering, the need to effectively join these materials becomes imperative. In many instances, the two specified alloys can be joined to produce new structures [25–27]. Further development of friction stir processing (FSP) in welded joints necessitates comprehensive research on various distinct welded joints.

The aforementioned literature review uncovered very few works that discuss the impact of FSP on TIG welding of dissimilar heat-treatable aluminium alloys. In the present investigation, an attempt was made to enhance the tensile strength, impact toughness, and wear resistance of the TIG-welded dissimilar AA6061-T6/AA7075-T6 weldments by utilizing FSP. Improving the mechanical and microstructural features of tungsten inert gas welded joints through friction stir processing played a pivotal role in the field of design and manufacturing. The tungsten inert gas welding followed by friction stir processing aids in the identification of the optimal conditions for achieving quality joints. The optimal conditions were determined in the current investigation through the utilization of mechanical and microstructural characterization methods. The microstructural analysis of weldments facilitates a deeper understanding of structural modifications such as grain size variations, grain morphology, and precipitate distributions resulting from friction stir processing. The microstructural analyses were carried out through optical microscopy (OM), scanning electron microscopy (SEM), and energy diffraction scanning (EDS). Furthermore, SEM

Table 1 Element compositions (weight %) of the base alloys and filler wire metal

Metals	Cu	Zn	Mg	Mn	Cr	Ti	Fe	Si	Al
AA7075-T6	1.19	5.21	2.21	0.02	0.29	0.06	0.39	0.44	Balance
AA6061-T6	0.23	0.24	0.94	0.10	0.05	0.14	0.69	0.65	Balance
ER5356	0.015	0.03	4.78	0.15	0.12	0.08	0.13	0.02	Balance

Table 2 Mechanical and wear properties of the base AA6061-T6 and AA7075-T6 plates

Plates	σ_{TS} (MPa)	δ_{pe} (%)	E_{IT} (J)	Δh_{WR} (μm)
AA7075-T6	519	11.8	19	65
AA6061-T6	324	21.3	26	78

σ_{TS} = maximum tensile strength; δ_{pe} = maximum elongation; E_{IT} = maximum impact toughness; Δh_{WR} = maximum wear rate

Table 3 Selected TIG welding parameters

Working parameter	Welding current (A)	Arc voltage (V)	Welding speed (mm/s)	Argon flow rate (lpm)
Description	148	20	1.3	19

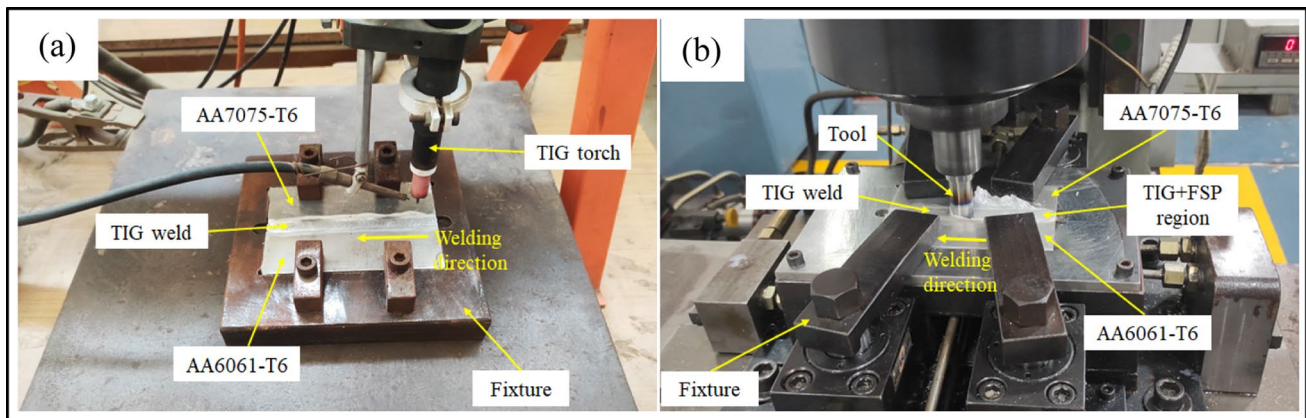
and spectroscopic analyses of tensile fractured surfaces were explored to validate the experimental findings.

2 Materials and methods

The high-strength aluminum AA6061-T6 and AA7075-T6 alloys used in the present study were cut into specific dimensions of $150 \times 50 \times 6 \text{ mm}^3$, were selected as the base alloys and ER 5356 [16, 24, 28] as the filler wire metal for TIG welding. Table 1 reported the elemental compositions of the

base alloys and filler wire metal obtained by energy diffraction scanning methods. The mechanical and wear features of the base alloys and TIG weldment with filler ER5356 were determined experimentally and presented in Table 2.

Table 3 displays the working process parameters for TIG welding of dissimilar aluminum plates based on relevant literatures [7, 17, 24] and lab experiments. However, the input FSP parameters viz. tool spindle speed, traverse speed, and tilt angle and their ranges were also identified through relevant literatures [10, 29, 30] and laboratory experiments. Before TIG welding, every plate's faying surface was thoroughly cleaned using acetone and a wire brush to eliminate oxide coatings and other impurities. Following the removal of oxide layers, V-grooves were machined with a 1.6 mm root gap, a 1.6 mm root face, and a 90° groove angle. A completely automatic TIG welding arrangement (KEMPP MasterTig 335 ACDC G) (Fig. 1a) was employed to fabricate TIG welded joints for the selected optimum welding parameters given in Table 3. Following a comprehensive cleaning process, both the aluminum plates were affixed to a mild steel platform measuring 200 mm by 200 mm, which had a thickness of 30 mm. Mechanical clamps were used to ensure a secure attachment and prevent distortion due to the welding heat [24]. During the TIG welding procedures, argon gas with a purity level of 99.99% was utilized along with an alternating current polarity. A double pass welding operation was carried out, employing a pure tungsten electrode of 3.2 mm in diameter, a 2.4 mm infill metal electrode, and a consistent arc gap of 2.5 mm.

**Fig. 1** Experimental setup of **a** an automatic TIG welding process, and **b** TIG + FSP welding technique

After the fabrication of TIG welded joints, FSP was carried out on the welded joints using a Computer Numerical Control (CNC) FSW machine (40kN HYD) as shown in Fig. 1b. Before FSP was used, the surfaces of both the base alloy were meticulously cleaned, and they were firmly placed onto an 8 mm-thick mild steel fixture that measured 285 mm in length and 177 mm in width. Mechanical clamps were then used to securely attach them. Additionally, the dedicated FSW machine is equipped with hydraulic clamps to avoid deformation caused by high forging pressure and enhanced welding temperatures owing to frictional heat. AA6061-T6 was positioned on the advancing side, whereas AA7075-T6 was positioned on the retreating side. One can observe that the advancing direction refers to the side where the rotational and traverse speed of the tool pin are in same direction, while the retreating side refers to side where the rotational and traverse speed of the tool pin are in opposite direction [31]. A tool constructed from H13 tool steel was employed during FSP operations. The tool had the following dimensions: shoulder diameter of 20 mm, pin length of 5.4 mm, and a 3 mm diameter at the tip and a 6 mm diameter at the base. The tapered square [32] pin profile tool was chosen for FSP operation as it yielded the best results with improved material mixing and no tunnel defects observed during trial experiments. The TIG + FSP experiments were conducted using the process parameters outlined in Table 4. Each experiment involved a single pass, a plunge depth of 0.5 mm, and a dwell time of 20 s. Figure 2 depicts the weld appearance of TIG and TIG + FSP welded joints, which disclose the formation of uniform ripples without any thermal cracks for TIG welds and the absence of any defects or

additional flash for TIG + FSP welds, indicating the successful fabrication of both types of joints.

Microstructural samples were taken from the weld region of TIG and TIG + FSP weldments using wire electric discharge machining (EDM). Afterward, the welded specimens underwent a thorough grinding and polishing process, starting with a 220-grit size and progressing up to 2200 grit size abrasive papers. Subsequently, they were subjected to diamond polishing using 0.5 μm grit size diamond paste and then etched with Keller's reagent for 12 s to achieve a mirror finish. The microstructural analysis was conducted using an optical microscope (Metzer-M, India) and scan electron microscope (Make: Zeiss SUPRA40) equipped with an EDS detector. Phase analysis was carried out utilizing an XRD machine (Empyrean, Malvern PANalytical diffractometer) with XRD data recorded at $\lambda = 1.5418 \text{ \AA}$ and 2θ ranges spanning from 10 to 90°, employing $\text{CuK}\alpha$ radiation. Tensile, impact, and dry sliding wear assessments were conducted on TIG and TIG + FSP weldments to gauge the resulting outcomes.

A transverse tensile test specimen was created through wire EDM, following the ASTM E8-M04 standard. Tensile examination utilized a Zwick/Roell Z250 universal testing equipment (as seen in Fig. 3a) with a 250 kN capacity, operating at a strain rate of 2 mm/min under usual circumstances. Charpy impact examination was performed utilizing a pendulum-style Tinius Olsen IT406 impact tester (as depicted in Fig. 3b) at usual circumstances. Charpy impact specimens adhered to ASTM E23-04 standards. In the assessment of impact toughness, parameters included an impact speed of 5.5 m/s, a pendulum mass of 27 kg, and an impacting angle of 90 degrees. Figure 3c and d provide a detailed depiction of the tensile and Charpy impact test specimens with their dimensional attributes. The pin-on-disc wear experiments were conducted in accordance with ASTM G99-05 using a high-temperature DUCOM TR-20L-PHM 800-DHM rotary tribometer under dry sliding conditions. Prismatic test samples, sized $5 \times 5 \times 10 \text{ mm}^3$, were extracted via wire EDM from the weld bead area and tested against an EN31 steel disk with a hardness of 63 HRC. After performing a thorough cleaning on the test samples and disc, the frictional

Table 4 Selected TIG + FSP welding parameters

Specimens	Tool traverse speed (mm/min)	Tool spindle speed (rpm)	Tool tilt angle (degree)
1	55	900	2
2		1100	
3		1300	

Fig. 2 Weld bead appearance of **a** TIG weldment, **b** TIG + FSP weldment (1300 rpm)

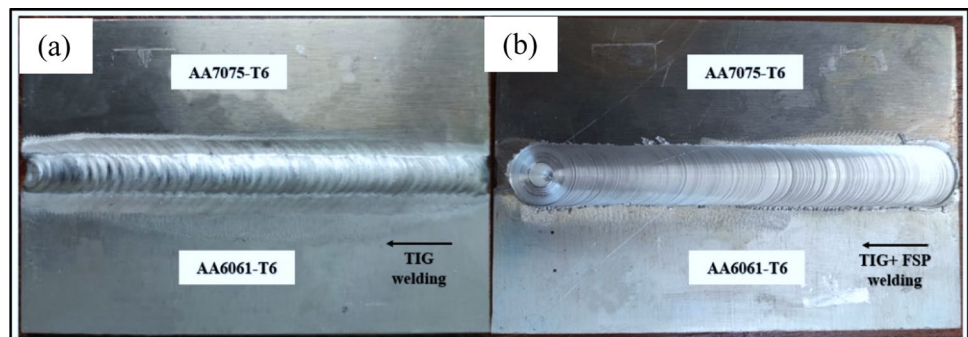
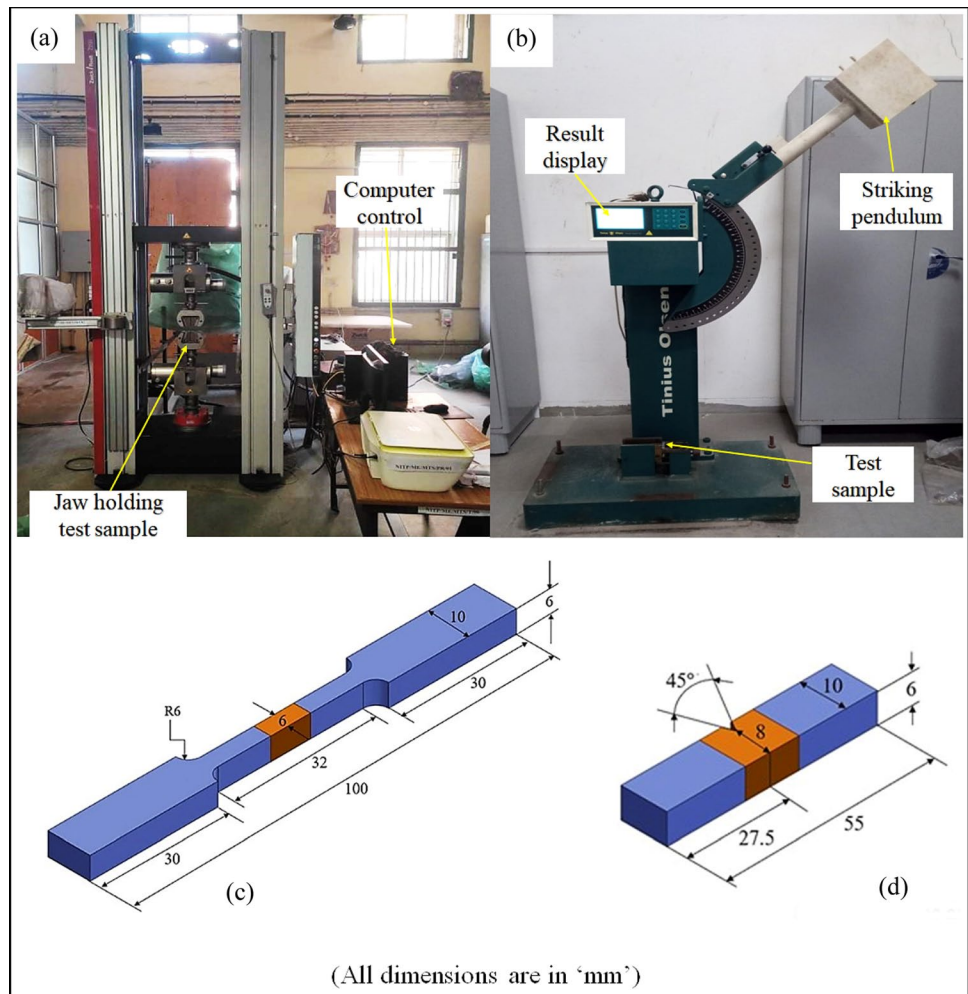


Fig. 3 **a** Universal testing machine for tensile test, **b** Tinius Olsen machine for Charpy impact test, **c** tensile sample, and **d** impact sample with proper dimensions



force between the pin and disc was measured using a stress sensor to estimate the coefficient of friction (COF). The tests were conducted under a vertical load of 40 N, with a track diameter of 40 mm, and disc rotation speeds of 450 rpm, 575 rpm, and 875 rpm, each lasting for 10 min. Optical microscopy was subsequently employed to examine the worn-out samples and investigate wear surface morphology. Three repetitions of each test, including the tensile, impact, and wear tests, were conducted in the current investigation, and the mean value of each test was recorded.

3 Results and discussion

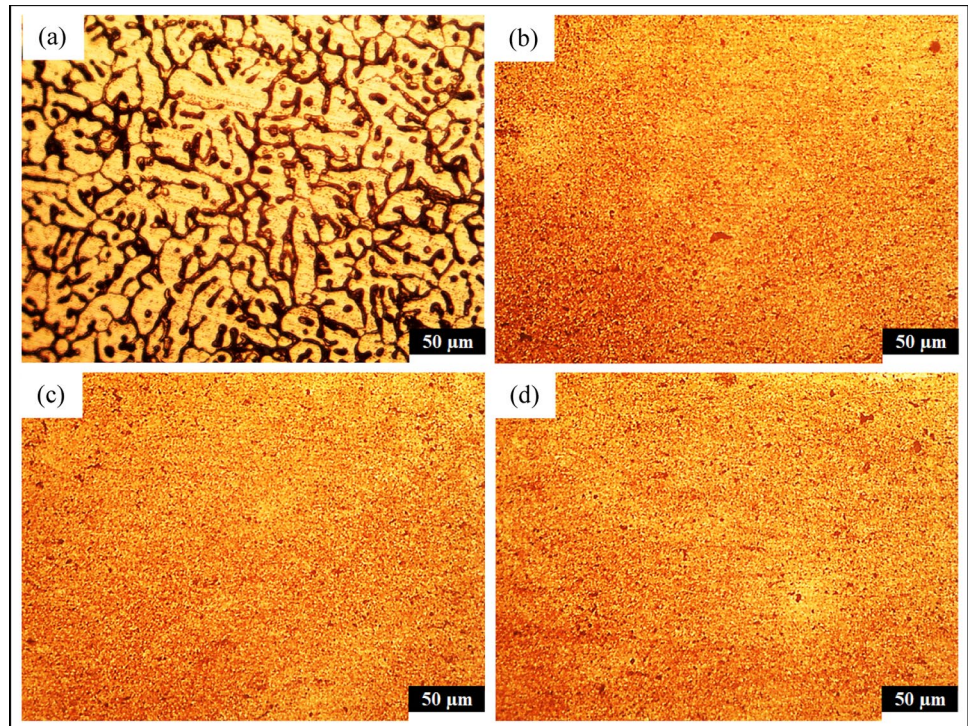
3.1 Microstructure

Figure 4 depicts the optical microstructures at the centre of unprocessed TIG and friction stir processed (TIG + FSP) joints. Fusion zone (FZ) refers to the middle of TIG welded connections, which is the distinct non-equilibrium cast micromorphology that emerges due to constitutional

undercooling and varied nucleation during rapid welding thermal cycles [33]. Figure 4a displays the TIG weld microstructure of the FZ at the weld centre which consists of dendritic grain morphology. Additionally, the ImageJ software was used to analyse the average grain size of TIG and TIG + FSP welded connections. According to the findings, the average grain size in the TIG weldment's fusion zone with filler ER5356 is approximately of 24.68 μm (see Fig. 4(a)). Since, the TIG welding involves local melting and solidification, leading to relatively higher heat concentrations and slower cooling rates near the weld, which result in dendritic structures, and coarser grains in the welded joints [24].

Figure 4b, c, and d display the TIG + FSP weld microstructure of the stir zone (SZ) at the weld nugget centre at different tool spindle speeds 900 rpm, 1100 rpm, and 1300 rpm. Results display that all the TIG + FSP welded samples exhibit fine equiaxed grain morphology at the centre of stir zone. It can be addressed that; the fusion welding process completely obliterates the dendrite structure after friction stir processing. Evidently, the FSP leads to

Fig. 4 Optical micrographs at the weld centre for **a** TIG welded joint, and TIG + FSP joint at **b** 900 rpm, **c** 1100 rpm, and **d** 1300 rpm

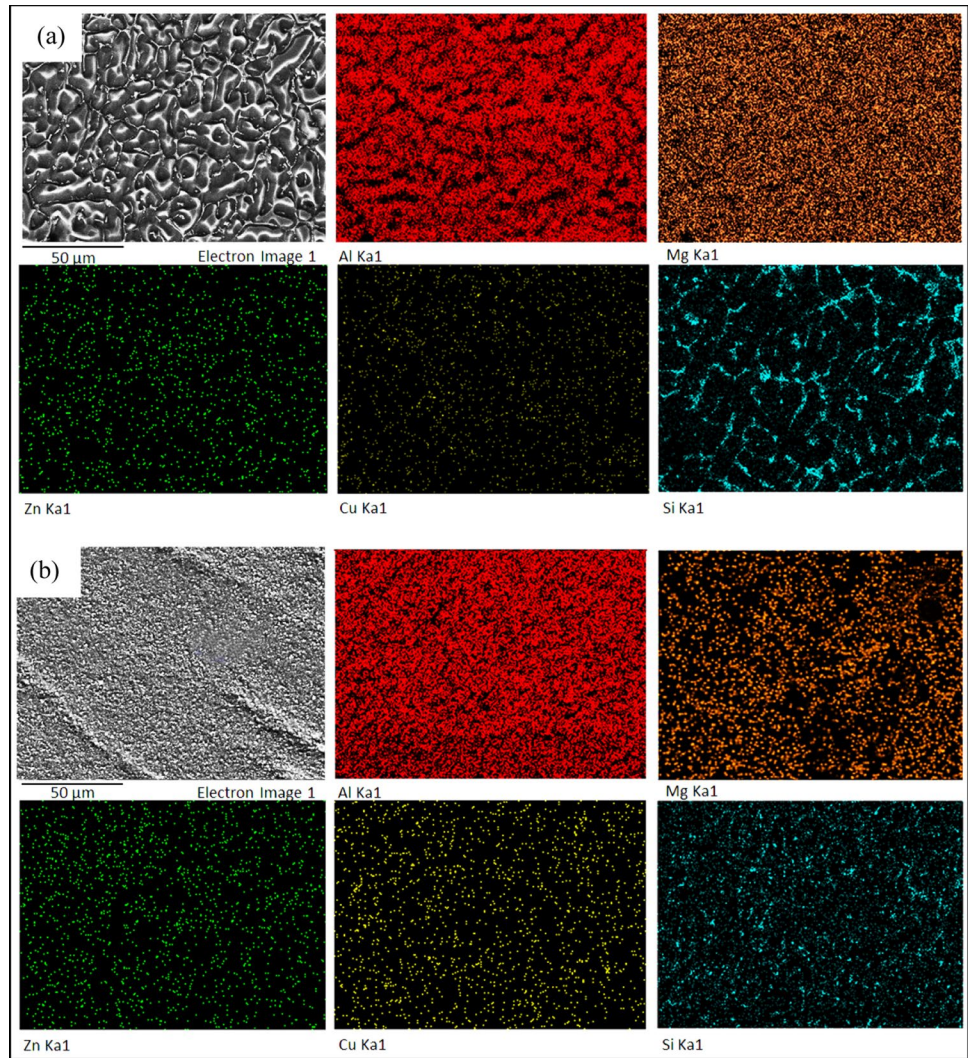


the formation of highly refined equiaxed grains, replacing the non-oriented larger grains that originated during solidification. The utilization of FSP induces notable heat due to friction and substantial plastic deformation, prompting dynamic recrystallization (DRX) within the SZ. This process results in the creation of uniform, finely-grained, and equiaxed recrystallized grains, as illustrated in Fig. 4b, c, and d. The friction stir modification leads to the formation of a SZ microstructure with grain sizes of 8.13 μm , 6.02 μm , and 4.17 μm at tool spindle speeds of 900 rpm, 1100 rpm, and 1300 rpm, respectively. As the tool spindle speed increases, the average particle size at the SZ decreases, which supports Mehdi and Mishra's findings [17]. An increased spindle speed value may result in significant frictional heat in the SZ, which may cause adequate heat generation and tool agitating action, resulting in the decreased average grain size [34]. It has been proven that different friction stir processing factors, such as tool profile, elemental composition, substrate temperature, vertical forging pressure, and active cooling, have an enormous impact on the size of recrystallized grains in the stirred zone [35]. FSP stands for a hot working technique. The concurrent occurrence of dynamic recovery, recrystallization, and grain growth is a result of substantial plastic deformation at elevated temperatures. Moreover, in metals like aluminium with elevated stacking fault energy, dislocation movement and slip occur more effortlessly during hot working, thus promoting dynamic recovery [36].

Figure 5 presents the SEM–EDS elemental mapping results for TIG and TIG + FSP weldments (1300 rpm) to

identify the intermetallic precipitates formation and their dispersion within the weld metal matrix or grain boundaries. SEM results reveal the presence of coarse dendritic grain microstructures in the fusion zone for the TIG welded joint (Fig. 5a) and a banding pattern emerges from the retreating side in the stirred zone [37], and the grain microstructure in this banding pattern is very fine for the TIG + FSP welded joint (Fig. 5b). Mechanical properties of TIG welds degrade due to the presence of coarse dendritic structures, whereas those of TIG + FSP welds increase due to the presence of fine equiaxed grains [35]. The elemental mapping results of the TIG and TIG + FSP welded joints reveal the presence of strengthening elements such as Mg, Zn, Cu, and Si along with Al. The existence of a considerable Mg, Zn and Cu along with Al in both the welded joints confirms the formation of significant intermetallic precipitates such as MgZn_2 and Al_2CuMg . Reyaz and Sinha [7] performed X-ray diffraction analysis and SEM–EDS analyses for the weld metal in FZ and found the similar intermetallic precipitates within the FZ of TIG welded dissimilar AA6061-T6/AA7075-T6 alloys. However, for the TIG + FSP welded joint, the distribution of alloying elements like Mg, Cu, Zn, and Si elements were lighter than the TIG welded joint and found to be uniformly distributed within the weld matrix and along the grain boundaries, as shown in Fig. 5a and b. This elucidates that the intermetallic precipitates were fragmented significantly in the weld metal after FSP [35, 37]. Thus, it can be concluded that post FSP of TIG weld strongly influences the microstructural characteristics, including grain structures,

Fig. 5 SEM–EDS elemental mapping at the weld centre for a TIG welded joint, and TIG + FSP joint at 1300 rpm



amount of intermetallic precipitates variations and defect formations, which may further affect the mechanical properties of the weldments.

3.2 Tensile strength

The tensile strength of a TIG welded dissimilar AA7075-T6/AA6061-T6 joint with ER5356 filler was shown to be

affected by FSP parameters including tool spindle speed. Table 5 displays the maximum tensile strength, percent elongation, joint efficiency, and fracture position of the TIG and TIG + FSP welded joints at different tool spindle speed. The joint efficiency [37] was calculated as the ratio of tensile strength of welded joint to the tensile strength of lower strength base alloy (in case of dissimilar metal welding). The maximum tensile strength, percent elongation, and joint

Table 5 Mechanical and wear characteristics of the TIG and TIG + FSP welded joints

Specimen	Spindle speed (rpm)	σ_{TS} (MPa)	δ_{pe} (%)	η_{Joint} (%)	Fracture position	E_{IT} (J)	Δh_{WR} (μm)
TIG Joint	–	159	8.4	49.07	Fusion zone	9	128
TIG + FSP Joint	900	210	13.1	64.81	HAZ of AA6061-T6	12	98
TIG + FSP Joint	1100	244	15.6	75.30	HAZ of AA6061-T6	15	84
TIG + FSP Joint	1300	278	19.8	85.80	HAZ of AA6061-T6	17	68

σ_{TS} = maximum tensile strength; δ_{pe} = maximum percent elongation; η_{Joint} = joint efficiency; E_{IT} = maximum impact toughness; Δh_{WR} = maximum wear rate

efficiency are the order of 278 MPa, 19.8%, and 85.80%, respectively for a tool spindle speed of 1300 rpm, while the minimum tensile strength, percent elongation, and joint efficiency are the order of 210 MPa, 13.1%, and 64.81%, respectively for a tool spindle speed of 900 rpm. Tensile strength of TIG + FSP joints is shown to improve with increasing spindle speed of the welding process. The flow of material in the stir zone (SZ) and the heat generated during the welding procedure affect the durability and strength of TIG + FSP weldments [38]. To achieve high quality joints, it's imperative to manage the movement of materials, thermal softening, heat generation, and material plasticity. The critical elements influencing material flow and heat production during the FSP method include the spindle speed and traverse speed. The traverse speed varies inversely with the heat produced, while the tool spindle speed changes proportionally to the heat input. An elevated spindle speed can lead to substantial frictional heat in the SZ, facilitating sufficient heat production and enabling effective tool stirring action for proper plastic deformation of the metal. This, in turn, enhances tensile strength [37]. Therefore, when the tool spindle speed is raised while keeping the traverse speed constant, the tensile strength of the joint is enhanced. It was determined that the tool spindle speed had a significant impact on the tensile characteristics of the FSW weldments [39]. The stress–strain graphs of the TIG + FSP weldments with different tool spindle speed is depicted in Fig. 6. The stress–strain graph for TIG weldments were also included for comparison and it can be seen that the all the TIG + FSP weldments produced a higher tensile strength than the TIG weldments. The joint efficiency of TIG welded joint is approximately 49%, while the joint efficiency for TIG + FSP weldment is approximately 85%. The primary factor determining a joint's characteristics

is its heat input, which governs the rate at which the weld metal cools and impacts the joint's strength. Porosity, coarse grain microstructures, thermal fractures, and dissolving of strengthening precipitates in the fusion zone are all problems often associated with TIG welded joints because of the high heat input concentrations required to melt the weld metal [7]. In contrast, TIG + FSP welded joints were found to exhibit extremely fine grain microstructures at the SZ and a disappearance of welding flaws in the FZ, including porosities and thermal fractures. Because to dynamic recrystallization (DRX), the SZ displayed a fine-grained, equiaxed structure [40]. Significant frictional heat generation and plastic strain during friction stir processing cause DRX in the SZ. In addition, the intensity of heat input concentration is lower in TIG + FSP welding than in TIG welding because the weld metal was not melted, resulting in ultrafine grains and enhanced tensile properties.

The transverse tensile specimens were fractured in the fusion zone (FZ) for the TIG welded joint and in the thermally affected zone (HAZ) for the TIG + FSP joint [37]. In contrast, in dissimilar aluminum alloys, the fusion-welded joints experienced failure at the FZ site, while friction stir-welded joints failed at the HAZ location [41, 42]. In addition, the tensile strength and ductility in the TIG and TIG + FSP welded joints exhibited a decrease compared to the base alloys, as indicated in Table 2 and 5. It was observed that these properties tended to improve with the precipitation hardening mechanism of the base alloys. The thermal properties of the base alloys played a crucial role in determining the strength and ductility of welds devoid of defects [16, 25]. Due to the localized melting and subsequent solidification caused by TIG welding, the diminished joint strength compared to the base alloys becomes apparent. During the TIG + FSP welding process, coarse grains formed within the grain boundary as a result of fine precipitates dissolving. This enhances the tensile strength of the welded joints, although it does not extend to the base alloys. The tensile properties of TIG and TIG + FSP welding processes differ from that of the base alloys due to microstructural changes involved in the welding processes.

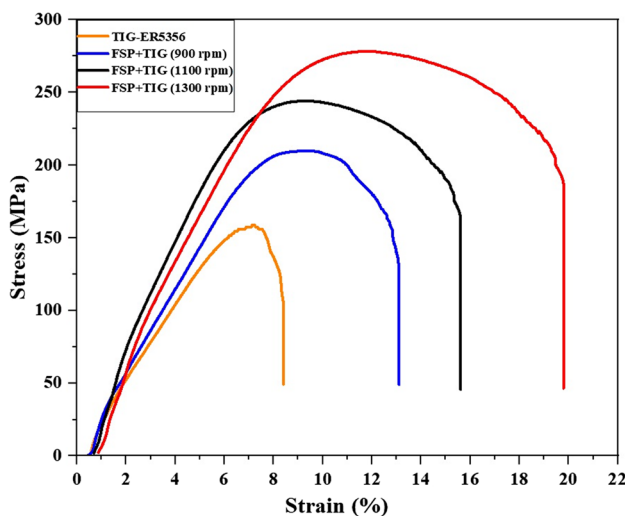


Fig. 6 Stress–strain graphs of TIG and TIG + FSP weldments at tool spindle speeds of 900 rpm, 1100 rpm, and 1300 rpm

3.3 Impact toughness

To assess the absorbed energy of TIG joints and TIG + FSP joints produced at different tool spindle speeds, impact examinations were conducted, and the findings are recorded in Table 5. The maximum impact toughness of the TIG + FSP joint is the order of 17 J for a tool spindle speed of 1300 rpm, while the minimum impact toughness of the TIG + FSP joint is the order of 12 J for a tool spindle speed of 900 rpm. The Charpy impact energy absorbed by the TIG + FSP joints is shown to improve with increasing spindle speed. It can be investigated that as the tool spindle speed

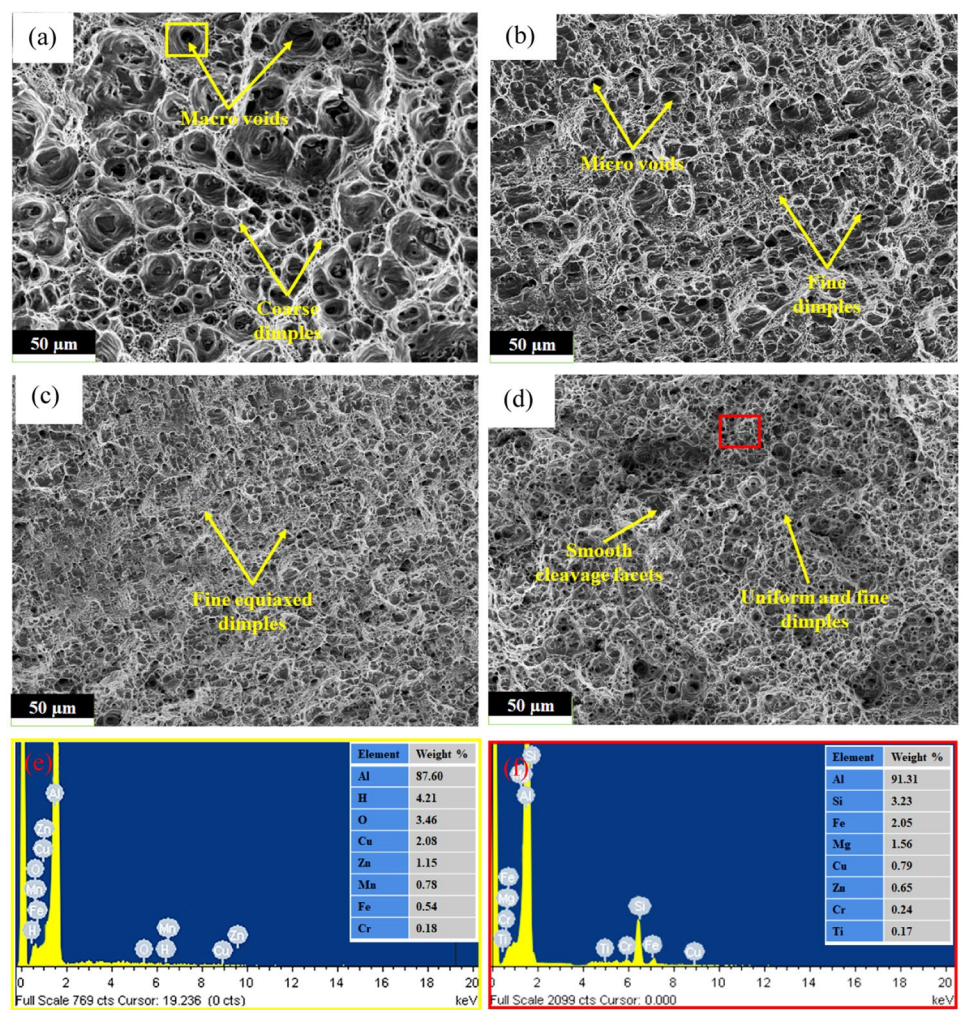
is increased the impact toughness of the joint is increased proportionally as can be seen in Fig. 7. Increasing the tool spindle speed can lead to increased heat generation due to higher frictional forces [18]. This can result in greater plastic deformation and better material flow in the stir region. As a result, the finer grain structure and improved metallurgical bonding may enhance the impact toughness of the joint [35]. The Charpy impact toughness of TIG weldment is of the order of 9 J, while the impact toughness for TIG + FSP weldment is of the order of 17 J (at 1300 rpm). The reduced impact toughness values in the TIG-welded joints compared to the TIG + FSP-welded joint can be attributed to several factors. These include the coarsening of grains within the fusion zone (FZ) due to the concentrated heat input during the fusion process, the dissolution of Guinier–Preston (GP) zones as a result of localized heating and melting in the FZ, the transformation of strengthening intermetallic precipitates such as $MgZn_2$ into less strengthening ones like Mg_2Al_3 , $Al_{32}Zn_{49}$, and Al_2Cu , and the presence of voids within the FZ. On the contrary, when it comes to TIG + FSP welded joints, applying friction stir processing significantly

raised the absorbed impact energy, even though both TIG and TIG + FSP joints exhibited lower impact toughness compared to the base alloys. FSP induces severe plastic deformation and dynamic recrystallization (DRX) through thermo-mechanical action, leading to improved material blending and finer microstructures within the stirring zone [36, 37]. In addition, FSP can cause uniform dispersion of precipitates, fragmentation of precipitates or dissolution of some precipitates across the GBs during DRX, significant strain hardening, and reduced defects such as voids or thermal cracks [36]. The combined effects of these factors contribute to a stronger microstructure of the processed zone, resulting in improved overall mechanical features, including impact toughness of the joint.

3.4 Fracture morphology

Figure 7 displays SEM images of fractured surfaces due to tension in TIG and TIG + FSP welded connections at varying tool spindle speeds. To confirm the insights obtained from fractography, energy Diffraction Scanning (EDS)

Fig. 7 SEM images of tensile fractured surfaces of **a** TIG joint, and TIG + FSP joints at tool spindle speed of **b** 900 rpm, **c** 1100 rpm, and **d** 1300 rpm; EDS analysis of marked square regions of fractured surfaces of **e** TIG joint and **f** TIG + FSP joint (1300 rpm)



analyses were conducted. In all TIG + FSP welded connections, cracks appeared in the thermally-affected zone (HAZ) of the AA6061-T6 side, whereas TIG welded connections exhibited damage in the fusion zone (FZ). The relationship between dimple size and weld joint strength and ductility is directly correlated. To put it differently, finer dimples lead to increased joint strength and ductility, while coarser dimples have the opposite effect [43]. On fractographic examination of TIG welded joints, a coarser dimple with some rough cleavage facets were observed. Some macro-voids were also existed within the fractured surfaces of the centre of fusion zone resulted in a brittle mode of failure (Fig. 7a). In contrast, on fractographic examination of TIG + FSP welded joints, all the joints displayed a fine and equiaxed dimples with no any voids. However, some micro-voids were also existed within the fractured surfaces of the thermally affected zone resulted in a ductile mode of failure (Figs. 7b–d). One can note that, as the tool spindle rises, the tensile fractured surfaces exhibit finer dimples, which supports the findings reported in Sect. 3.2. Energy diffraction scanning (EDS) examination of the void region marked as yellow square region, reveals the presence of 0.78% Mn, 4.21% H, 3.46% O, 2.08% Cu, 1.15% Zn, 0.18% Cr, and 0.54% Fe along with aluminum (Fig. 7e). The quick rate of cooling related to TIG welding leads to void formation in the FZ. During TIG welding, hydrogen can get trapped in the molten pool attributed to its fast-cooling rate leading to the formation of these voids in the FZ. Additionally, the difference in hydrogen dissolvability between aluminum alloy's liquid and solid states is accountable for the formation of hydrogen-induced voids [44]. Hydrogen is mainly derived from moisture and the moisture was mainly derived from the atmosphere, the base metals, the electrodes and the filler wire [45]. The moisture may enter into the weld pool from the rear of the plate as they were not shielded by argon and may cause oxygen inclusions in the weld. These voids serve as a stress concentrators and crack initiation sites, thereby degrading the overall integrity of the weld joint and responsible for the brittle fracture in the FZ [24]. An examination of the designated red square area using EDS analysis reveals the existence of 1.56% Mg, 3.23% Si, 0.79% Cu, 0.65% Zn, 0.65% Zn, 0.24% Cr and 0.17% Ti in addition to aluminum (Fig. 7f). The presence of notable quantities of Mg and Si serves as confirmation for the development of intermetallic precipitates like Mg_2Si , indicating their presence on the fracture surfaces of AA6061-T6. During FSP these intermetallic precipitates provides sufficient strength to the joint due to precipitation hardening mechanism. Therefore, during tensile test TIG + FSP joints showed significant necking before failure and responsible for the ductile fracture mode in the HAZ of AA6061-T6 side.

3.5 Wear rate

Drying slide experiments were performed to determine the rate of wear rate in terms of height (in microns) of TIG joints and TIG + FSP joints fabricated at different tool spindle speeds. The findings are recorded in Table 5. The maximum wear rate of the TIG + FSP welded joint is the order of 110 μm for a tool spindle speed of 900 rpm, while the minimum wear rate of the TIG + FSP joint is the order of 86 μm for a tool spindle speed of 1300 rpm. As obvious as it seems, as the value of the spindle speed is increased, the magnitude of wear rate of the TIG + FSP weldment decreased significantly. Consequently, as the tool spindle speed increased, the TIG + FSP weldment exhibited enhanced wear resistance. The decrease in wear rate value can be credited to significant grain refinement and enhanced material mixing within the SZ as a result of the ample generation of frictional heat during the friction stir processing [46, 47]. In addition, the wear rate of TIG welded joint is of the order of 132 μm , while the wear rate for TIG + FSP welded joint is of the order of 86 μm (at 1300 rpm). These findings align with earlier studies [37, 46].

Figure 8 presents the relationship between the coefficient of friction (COF) and the disc rotation speeds in both the TIG and TIG + FSP joints at a vertical load of 40 N. As the disc rotation speed is increased the coefficient of friction (COF) for both the TIG and TIG + FSP joints is decreased. Higher disc rotation speeds usually lead to more heat being generated. As the temperature increases, the pin and disc surfaces can become smoother, reducing roughness and the coefficient of friction (COF). Additionally, when the rotation speeds increase, the material undergoes increased shear and plastic deformation. This can result in smoother surfaces,

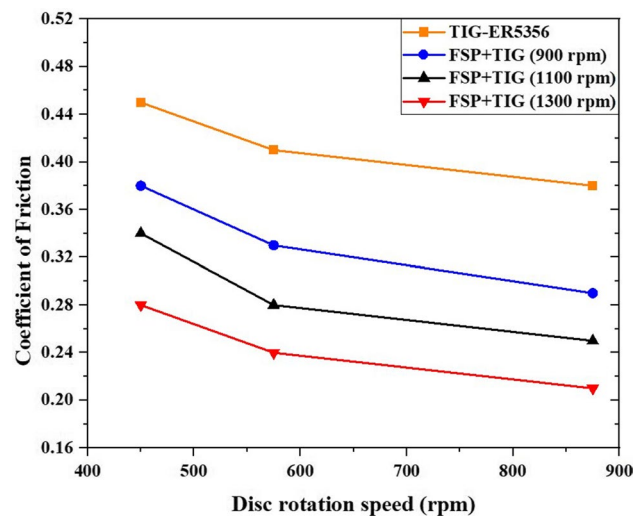


Fig. 8 Variation of coefficient of friction (COF) to disc rotation speeds of TIG and TIG + FSP joints

which can further reduce the COF. Figure 9 displays the correlation between the coefficient of friction (COF) and the sliding distance in both the TIG and TIG + FSP joints under a vertical load of 40 N. It was estimated that the average COF for TIG joint was 0.44. In contrast, the average COF of the TIG + FSP joints was approximately 0.38 at tool

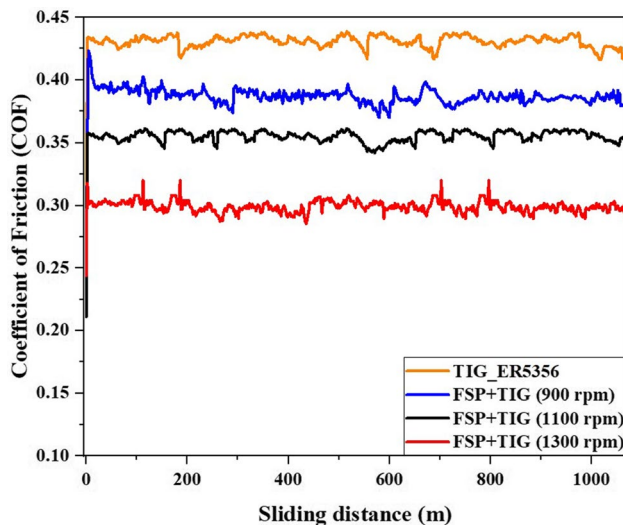
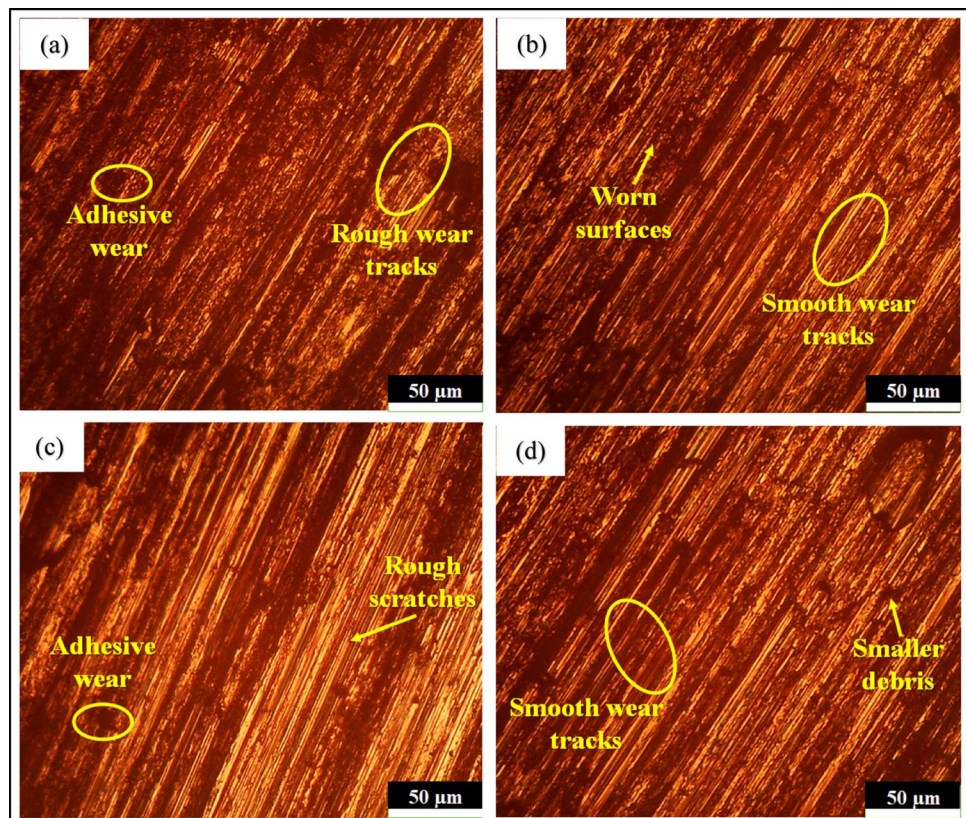


Fig. 9 Variation of coefficient of friction (COF) to the sliding distance of TIG and TIG + FSP joints

spindle speed of 900 rpm and 0.35 at tool spindle speed of 1100 rpm, and 0.32 at spindle speed of 1300 rpm. Higher tool rotation speeds can cause the weld material near the stir region to soften due to increased heat generation. Softer materials have lower COF because they deform easily when a load is applied, which decreases the resistance to motion, and thereby increasing the wear resistance of the joint. The results also demonstrated that the COF for TIG joints varies more with sliding distance than for TIG + FSP joints.

Figure 10 displays optical micrographs of the corroded surfaces of the TIG and TIG + FSP weldments under a 40 N vertical load. As depicted in Fig. 10a, the optical micrographs of the eroded surfaces of the TIG-weldment reveal superficial and irregular wear tracks attributable to a higher COF due to increased attrition from detritus and asperities on the hard counter particles. These traits may be traced back to the accumulation of loosely bound particles in the wear zone around TIG welded joints, which are dislodged during the sliding movement [7]. Adhesion wear, in which one surface region ploughs and clings to another, was identified as the dominant wear process. This adhesion is caused by the significant heat generated by friction during a dry sliding wear test [48]. These characteristics can be attributed to the dislodging of loosely bonded elements and accumulating in the wear zone as a result of the sliding action. In contrast, the eroded detritus observed in the TIG joints

Fig. 10 OM showing worn-out surfaces of **a** TIG joint, and TIG + FSP joints at tool spindle speed of **b** 900 rpm, **c** 1100 rpm, and **d** 1300 rpm



resembled microchips. The formation of these microchips most likely resulted from the oxidized coating peeling off during the wear examination. The presence of deteriorated detritus in TIG + FSP joints is significantly less than in TIG joints (Fig. 10b–d). Moreover, as the tool spindle speed rises, the uneven marks become smooth and uniform, signifying a higher level of plastic deformation and lower attrition during the wear test [25]. Abrasive wear particles are produced when the wear pin comes into contact with the disc material during dry sliding wear tests. At higher speeds, the abrasive wear particles can be better spread across the surface, reducing their impact on creating more scratches and decreasing friction and debris formation. Based on the observations mentioned, it can be concluded that TIG joints typically have more debris in the wear area and show rough wear tracks. In contrast, the wear section of TIG + FSP joints showed no signs of chipping and instead had smooth wear tracks. This indicates that TIG + FSP joints with a tool spindle speed of 1300 rpm showed better wear resistance than the other weldments. These results align with earlier research investigations [37, 49].

4 Conclusions

In this investigation, distinct AA6061-T6 and AA7075-T6 plates underwent butt-welding through automated TIG welding. Subsequently, FSP was applied to the TIG weldments at different tool spindle speeds to enhance the tensile strength, impact toughness, and wear resistance of the TIG-welded joints. To confirm the experimental findings, optical microscopy (OM), scanning electron microscopy (SEM), and energy diffraction scanning (EDS) on both TIG and TIG + FSP joints were carried out. The results of this research yielded the subsequent noteworthy conclusions:

1. The tensile strength and impact toughness of TIG-welded joints increased by 74.84% and 88.89%, respectively, after FSP treatment, while the wear rate decreased by 46.87% at a tool spindle speed of 1300 rpm. The joint strength and wear resistance were improved with increased spindle speeds, since they provide adequate frictional heat and plastic deformation across the SZ resulted in an improved material flow.
2. Microstructural analysis revealed that the TIG joint exhibited a dendritic grain morphology at the FZ centre, with an average grain size of 24.68 μm , while the TIG + FSP joint at 1300 rpm exhibited a of fine equiaxed grains, with an average grain size of 4.17 μm . Thus, TIG + FSP welding process resulted in improved joint properties due to ultrafine grains with fine equiaxed grains.

3. The TIG + FSP joint had a maximum tensile strength of 278 MPa, an impact toughness of 17 J, and a minimum wear rate of 86 μm at a tool spindle speed of 1300 rpm. In comparison, the TIG welded joint with filler ER5356 only had a maximum strength of 159 MPa, an impact toughness of 9 J, and a minimum wear rate of 132 μm .
4. The tensile fractured surface of TIG joints was featured by rough cleavage facets, coarse dimples with reasonable voids, resulting in a brittle fracture behaviour. However, the TIG + FSP joints exhibited the fine equiaxed dimples fractured surface with no voids, leading to a ductile fracture behaviour.
5. The worn-out surfaces of TIG joints was featured by rough wear tracks with larger debris voids resulted in a higher coefficient of friction. However, the TIG + FSP joints exhibited the uniform and smooth wear tracks with smaller debris resulted in a lower coefficient of friction and responsible for improved wear resistance.

Acknowledgements The authors extend their heartfelt appreciation to Prof. Qasim Murtaza from the Department of Mechanical Engineering at Delhi Technological University, Delhi, for providing the experimental setup and his lab support that significantly contributed to the successful completion of this research.

Author contributions MSBR: investigation, conceptualization, methodology, lab experiments, data collection, writing–original draft, review & editing. ANS: methodology, investigation, supervision.

Funding Not applicable.

Declarations

Conflict of interest The authors declare that they have no known competing financial interests or personal relationships that could have appeared to influence the work reported in this paper.

References

1. Mishra, R.S., Mahoney, M.W.: Friction stir processing: a new grain refinement technique to achieve high strain rate superplasticity in commercial alloys. *Mater. Sci. Forum.* **357–359**, 507–514 (2001). <https://doi.org/10.4028/www.scientific.net/MSF.357-359.507>
2. Raja, S., Muhamad, M.R., Jamaludin, M.F., Yusof, F.: A review on nanomaterials reinforcement in friction stir welding. *J. Market. Res.* **9**, 16459–16487 (2020). <https://doi.org/10.1016/j.jmrt.2020.11.072>
3. Raja, S., Muhamad, M.R., Yusof, F., Jamaludin, M.F., Suga, T., Liu, H., Morisada, Y., Fujii, H.: Friction stir alloying of AZ61 and mild steel with Al-CNT additive. *Sci. Technol. Weld. Join.* **27**, 533–540 (2022). <https://doi.org/10.1080/13621718.2022.2080449>
4. Senthilkumar, R., Prakash, M., Arun, N., Jeyakumar, A.A.: The effect of the number of passes in friction stir processing of aluminum alloy (AA6082) and its failure analysis. *Appl. Surf. Sci.* **491**, 420–431 (2019). <https://doi.org/10.1016/j.apsusc.2019.06.132>

5. Dieguez, T., Burgueño, A., Svoboda, H.: Superplasticity of a friction stir processed 7075–T651 aluminum alloy. *Proc. Mater. Sci.* **1**, 110–117 (2012). <https://doi.org/10.1016/j.mspro.2012.06.015>
6. Mishra, R.S., Ma, Z.Y.: Friction stir welding and processing. *Mater. Sci. Eng. R. Rep.* **50**, 1–78 (2005). <https://doi.org/10.1016/j.mser.2005.07.001>
7. Bin Reyaz, M.S., Sinha, A.N.: An experimental investigation on mechanical characteristics and wear behaviour of TIG welded dissimilar aluminum alloys. *J. Adhes. Sci. Technol.* (2023). <https://doi.org/10.1080/01694243.2023.2251782>
8. Iqbal, M.P., Vishwakarma, R.K., Pal, S.K., Mandal, P.: Influence of plunge depth during friction stir welding of aluminum pipes. *Proc. Inst. Mech. Eng. B J. Eng. Manuf.* **237**, 2085–2096 (2023). <https://doi.org/10.1177/09544405240949754>
9. Mehdi, H., Mabuwa, S., Msomi, V., Saxena, K.K.: Influence of friction stir processing on the mechanical and microstructure characterization of single and double V-groove tungsten inert gas welded dissimilar aluminum joints. *J. Mater. Eng. Perform.* (2022). <https://doi.org/10.1007/s11665-022-07659-7>
10. Salah, A.N., Mabuwa, S., Mehdi, H., Msomi, V., Kaddami, M., Mohapatra, P.: Effect of multipass FSP on Si-rich TIG welded joint of dissimilar aluminum alloys AA8011-H14 and AA5083-H321: EBSD and microstructural evolutions. *Silicon* **14**, 9925–9941 (2022). <https://doi.org/10.1007/s12633-022-01717-4>
11. Iqbal, M.P., Jain, R., Pal, S.K., Mandal, P.: Numerical modelling of friction stir welding of pipes: effect of tool shoulder on mechanical property and metallurgical characterization. *J. Manuf. Process.* **79**, 326–339 (2022). <https://doi.org/10.1016/j.jmapro.2022.04.028>
12. Iqbal, M.P., Jain, R., Pal, S.K.: Numerical and experimental study on friction stir welding of aluminum alloy pipe. *J. Mater. Process. Technol.* **274**, 116258 (2019). <https://doi.org/10.1016/j.jmatprotec.2019.116258>
13. Saini, N., Pandey, C., Dwivedi, D.K.: Ductilizing of cast hypereutectic Al–17%Si alloy by friction stir processing. *Proc. Inst. Mech. Eng. Part E J. Process Mech. Eng.* **232**, 696–701 (2018). <https://doi.org/10.1177/0954408917737735>
14. Alam, M.P., Sinha, A.N.: Effect of heat assisting backing plate in friction stir welding of high strength Al–Li alloy. *Energy Sources Part A: Recovery Utilization Environ. Eff.* **44**, 2851–2862 (2022). <https://doi.org/10.1080/15567036.2019.1651793>
15. Wu, B., Ibrahim, M.Z., Raja, S., Yusof, F., AbdulRazak, B., Muhamad, M.R.B., Huang, R., Zhang, Y., Badruddin, I.A., Hussien, M., Kamangar, S.: The influence of reinforcement particles friction stir processing on microstructure, mechanical properties, tribological and corrosion behaviors: a review. *J. Mater. Res. Technol.* **20**, 1940–1975 (2022). <https://doi.org/10.1016/j.jmrt.2022.07.172>
16. Mehdi, H., Mishra, R.S.: Microstructure and mechanical characterization of tungsten inert gas-welded joint of AA6061 and AA7075 by friction stir processing. *Proc. Inst. Mech. Eng. Part L: J. Mater. Des. Appl.* **235**, 2531–2546 (2021). <https://doi.org/10.1177/14644207211007882>
17. Mehdi, H., Mishra, R.S.: Investigation of mechanical properties and heat transfer of welded joint of AA6061 and AA7075 using TIG+FSP welding approach. *J. Adv. Join. Process.* **1**, 100003 (2020). <https://doi.org/10.1016/j.jajp.2020.100003>
18. Mehdi, H., Mishra, R.S.: An experimental analysis and optimization of process parameters of AA6061 and AA7075 welded joint by TIG+FSP welding using RSM. *Adv. Mater. Process. Technol.* **8**, 598–620 (2022). <https://doi.org/10.1080/2374068X.2020.1829952>
19. Thakral, R., Sharma, S., Singh, T.: Experimental analysis of friction stir processing of TIG welded aluminium alloy 6061. *IJRST-Int. J. Innov. Res. Sci. Technol.* **4**, 1–7 (2018)
20. da Silva, J., Costa, J.M., Loureiro, A., Ferreira, J.M.: Fatigue behaviour of AA6082-T6 MIG welded butt joints improved by friction stir processing. *Mater. Des.* **51**, 315–322 (2013). <https://doi.org/10.1016/j.matdes.2013.04.026>
21. Abdul Hammied Saad, N., Abass Hashim, D.: Using friction stir process (FSP) to improve the properties of AA7020 aluminum alloy weldments welded by tungsten inert gas (TIG). (الاحتكاكي بال AA720) (اللومنيوم ملحومات خواص لتحسين FSP الخلط عملية استخدام المحمي الكهربائي القوس لحام بطريقة الملحومة) (الخامل غاز TIG). (2015)
22. Fuller, C.B., Mahoney, M.W.: The effect of friction stir processing on 5083–H321/5356 Al arc welds: microstructural and mechanical analysis. *Metall. Mater. Transa. A* **37**, 3605–3615 (2006)
23. Hakem, M., Lebaili, S., Mathieu, S., Miroud, D., Lebaili, A., Cheniti, B.: Effect of microstructure and precipitation phenomena on the mechanical behavior of AA6061-T6 aluminum alloy weld. *Int. J. Adv. Manuf. Technol.* **102**, 2907–2918 (2019). <https://doi.org/10.1007/s00170-019-03401-1>
24. Bin Reyaz, M.S., Sinha, A.N.: Analysis of mechanical properties and optimization of tungsten inert gas welding parameters on dissimilar AA6061-T6 and AA7075-T6 by a response surface methodology-based desirability function approach. *Eng. Optim.* (2023). <https://doi.org/10.1080/0305215X.2023.2230133>
25. Mehdi, H., Mishra, R.S.: Influence of friction stir processing on weld temperature distribution and mechanical properties of TIG-welded joint of AA6061 and AA7075. *Trans. Indian Inst. Met.* **73**, 1773–1788 (2020). <https://doi.org/10.1007/s12666-020-01994-w>
26. Mehdi, H., Mishra, R.S.: Effect of friction stir processing on microstructure and mechanical properties of TIG welded joint of AA6061 and AA7075. *Metall. Microstruct. Anal.* **9**, 403–418 (2020). <https://doi.org/10.1007/s13632-020-00640-7>
27. Mehdi, H., Mishra, R.S.: Effect of friction stir processing on mechanical properties and heat transfer of TIG welded joint of AA6061 and AA7075. *Def. Technol.* **17**, 715–727 (2021). <https://doi.org/10.1016/j.dt.2020.04.014>
28. Ishak, M., Mohd Noordin, N.F., Ahmad Shah, L.H.: Feasibility study on joining dissimilar aluminum alloys AA6061 and AA7075 by tungsten inert gas (TIG). *J. Teknol.* **75**, 79 (2015). <https://doi.org/10.11113/jt.v75.5177>
29. Ma, Z.Y.: Friction stir processing technology: a review. *Metall. Mater. Trans. A.* **39**, 642–658 (2008). <https://doi.org/10.1007/s11661-007-9459-0>
30. Yang, Y., Zhao, Y., Kai, X., Tao, R.: Superplasticity behavior and deformation mechanism of the in-situ Al₃Zr/6063Al composites processed by friction stir processing. *J. Alloys Compd.* **710**, 225–233 (2017). <https://doi.org/10.1016/j.jallcom.2017.03.246>
31. Liyakat, N.A., Veeman, D.: Improvement of mechanical and microstructural properties of AA 5052–H32 TIG weldment using friction stir processing approach. *J. Market. Res.* **19**, 332–344 (2022). <https://doi.org/10.1016/j.jmrt.2022.05.015>
32. Jamshidi Aval, H.: Influences of pin profile on the mechanical and microstructural behaviors in dissimilar friction stir welded AA6082-AA7075 butt joint. *Mater Des.* **67**(413), 421 (2015)
33. Song, G., Wang, Z., Liu, Z., Liu, L.: Effect of partial rolling on the microstructure and mechanical properties of laser-TIG hybrid welded joints of 7075–T6 aluminum alloy. *Int. J. Adv. Manuf. Technol.* **121**, 589–599 (2022). <https://doi.org/10.1007/s00170-022-09287-w>
34. Li, Y., Sun, D., Gong, W.: Effect of tool rotational speed on the microstructure and mechanical properties of bobbin tool friction stir welded 6082–T6 aluminum alloy. *Metals (Basel)* **9**, 894 (2019). <https://doi.org/10.3390/met9080894>
35. Shamanian, M., Mostaan, H., Safari, M., Szpunar, J.A.: Friction stir modification of GTA 7075–T6 Al alloy weld joints: EBSD study and microstructural evolutions. *Archiv. Civ. Mech. Eng.* **17**, 574–585 (2017). <https://doi.org/10.1016/j.acme.2017.01.002>

36. Roen, G.A., Yousefi, S.G., Emadi, R., Shooshtari, M., Lotfian, S.: Remanufacturing the aa5052 gtaw welds using friction stir processing. *Metals (Basel)* **11**, 749 (2021). <https://doi.org/10.3390/met11050749>
37. Mehdi, H., Mishra, R.S.: Effect of friction stir processing on mechanical properties and wear resistance of tungsten inert gas welded joint of dissimilar aluminum alloys. *J. Mater. Eng. Perform.* **30**, 1926–1937 (2021). <https://doi.org/10.1007/s11665-021-05549-y>
38. Karthikeyan, M.: Effect of tool travel speed on tensile strength of friction stir welded dissimilar joint of aluminium AA6061 T6 alloy and maraging M250 steel. *Mater. Res. Express.* **8**, 026508 (2021). <https://doi.org/10.1088/2053-1591/abde57>
39. Simar, A., Bréchet, Y., de Meester, B., Denquin, A., Gallais, C., Pardoën, T.: Integrated modeling of friction stir welding of 6xxx series Al alloys: process, microstructure and properties. *Prog. Mater. Sci.* **57**, 95–183 (2012). <https://doi.org/10.1016/j.pmatsci.2011.05.003>
40. Roen, G.A., Yousefi, S.G., Emadi, R., Shooshtari, M., Lotfian, S.: Remanufacturing the AA5052 GTAW welds using friction stir processing. *Metals (Basel)* **11**, 749 (2021). <https://doi.org/10.3390/met11050749>
41. Koilraj, M., Sundareswaran, V., Vijayan, S., Koteswara Rao, S.R.: Friction stir welding of dissimilar aluminum alloys AA2219 to AA5083—optimization of process parameters using Taguchi technique. *Mater. Des.* **42**, 1–7 (2012). <https://doi.org/10.1016/j.matdes.2012.02.016>
42. Koli, Y., Yuvaraj, N., Aravindan, S., Vipin: CMT joining of AA6061-T6 and AA6082-T6 and examining mechanical properties and microstructural characterization. *Trans. Indian Inst. Metals* **74**, 313–329 (2021). <https://doi.org/10.1007/s12666-020-02134-0>
43. Peng, D., Shen, J., Tang, Q., Wu, C.P., Zhou, Y.B.: Effects of aging treatment and heat input on the microstructures and mechanical properties of TIG-welded 6061–T6 alloy joints. *Int. J. Miner. Metall. Mater.* **20**, 259–265 (2013). <https://doi.org/10.1007/s12613-013-0721-8>
44. Dwivedi, D.K.: Welding metallurgy metallurgical aspect of metal joining. *Process. Fundam. Metal Join. Process. Mech. Perform.* (2022). https://doi.org/10.1007/978-981-16-4819-9_20
45. Qin, Q., Zhao, H., Li, J., Zhang, Y., Zhang, B., Su, X.: Microstructures and mechanical properties of TIG welded Al-Mg₂Si alloy joints. *J. Manuf. Process.* **56**, 941–949 (2020). <https://doi.org/10.1016/j.jmapro.2020.05.058>
46. Abolusoro, O.P., Akinlabi, E.T.: Effects of processing parameters on mechanical, material flow and wear behaviour of friction stir welded 6101–T6 and 7075–T651 aluminium alloys. *Manuf. Rev.* **7**, 1 (2020). <https://doi.org/10.1051/mfreview/2019026>
47. Dragatogiannis, D.A., Koumoulos, E.P., Kartsonakis, I.A., Pantelis, D.I., Karakizis, P.N., Charitidis, C.A.: Dissimilar friction stir welding between 5083 and 6082 Al alloys reinforced with TiC nanoparticles. *Mater. Manuf. Process.* **31**, 2101–2114 (2016). <https://doi.org/10.1080/10426914.2015.1103856>
48. Butola, R., Tyagi, L., Singari, R.M., Murtaza, Q., Kumar, H., Nayak, D.: Mechanical and wear performance of Al/SiC surface composite prepared through friction stir processing. *Mater. Res. Express.* **8**, 016520 (2021). <https://doi.org/10.1088/2053-1591/abd89d>
49. Kumar, A., Das, A.K., Rai, P.K.: Tribological behaviour of Al–Ni–TiB₂ composite coating on AA1100 Al-alloy prepared using TIG torch welding route. *Trans. Indian Inst. Met.* **75**, 1899–1907 (2022). <https://doi.org/10.1007/s12666-021-02509-x>

Publisher's Note Springer Nature remains neutral with regard to jurisdictional claims in published maps and institutional affiliations.

Springer Nature or its licensor (e.g. a society or other partner) holds exclusive rights to this article under a publishing agreement with the author(s) or other rightsholder(s); author self-archiving of the accepted manuscript version of this article is solely governed by the terms of such publishing agreement and applicable law.